Inorganic Chemistry

Article

Cite This: *Inorg. Chem.* XXXX, XXX, XXX−XXX

pubs.acs.org/IC

Conductive Leaflike Cobalt Metal−Organic Framework Nanoarray on Carbon Cloth as a Flexible and Versatile Anode toward Both Electrocatalytic Glucose and Water Oxidation

Ziyi Wei,[†,⊥] Wenxin Zhu,[†,⊥] Yinge Li,[†] Yiyue Ma,[†] Jing Wang,[†] Na Hu,[‡] Yourui Suo,[‡]
and Jianlong Wang*,[†]

[†]College of Food Science and Engineering, Northwest A&F University, 22 Xinong Road, Yangling 712100, Shaanxi, China
[‡]Qinghai Key Laboratory of Qinghai-Tibet Plateau Biological Resources, Northwest Institute of Plateau Biology, Chinese Academy of Sciences, 23 Xinning Road, Xining 810008 Qinghai, China

Supporting Information

ABSTRACT: Transition metal−organic frameworks (MOFs), on account of their unique inherent properties of large pore volume, high specific surface area, tunable pores, and good catalytic activity, have been highly regarded as superior catalysts recently for water electrolysis, supercapacitors, batteries, sensors, and so on. Herein, we report on a cobalt MOF phase with 3D well-aligned nanosheets array architecture on carbon cloth (Co-MOF NS/CC), fabricated by a facile ambient liquid-phase deposition, could serve as a self-standing Janus catalytic electrode toward both glucose and water oxidation. It shows good glucose-sensing performance with low determination limit and large detection range. Also, it exhibits high water-oxidation efficiency with low overpotential and good durability. This work demonstrates the potential of utilizing transition-metal based well-aligned MOF nanoarrays for electrocatalytic oxidation.

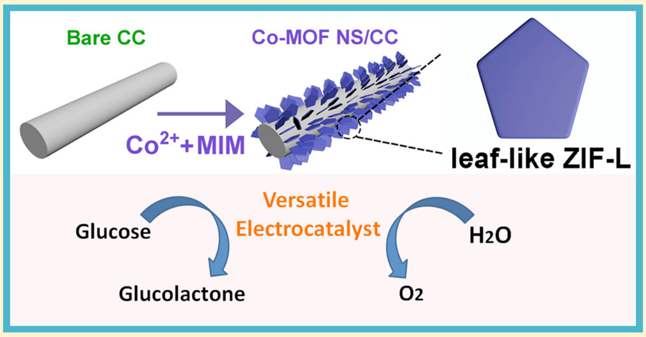

■ INTRODUCTION

Diabetes is a group of metabolic diseases characterized by high blood glucose, which will lead to systemic damage and dysfunction of tissues and organs, rapidly growing to a global epidemic.[1,2] The diagnosis and management of diabetes demands analysis of blood glucose level several times a day, which calls for the development of highly sensitive and efficient glucose sensors. Among different sensing methods, electrochemical glucose detection based on the principle of electrocatalytic glucose oxidation is highly regarded as an effective means.[3] Currently, commercial glucose sensing equipment is basically based on glucose oxidase (GOD)-assisted biorecognition and oxidation of glucose molecules in the global market.[4] In spite of the fact that enzyme-based glucose sensors have high sensitivity and excellent selectivity,[5] they suffer from some natural vulnerabilities like the high cost of the enzymes used, a complex enzyme-immobilization process, instability resulting from the denaturation of the enzymes, and low conductivity on account of indirect electron transfer.[1,4] By contrast, nonenzymatic glucose sensors based on direct electrocatalytic oxidation has received increasing attention due to their direct electron-transfer-shuttle-free sensing style.[5] This kind of sensors have attractive superiorities of high sensitivity, good reproducibility and low cost.[4,6] Although conventional nonenzymatic sensors based on the precious metals and their alloys have excellent glucose sensing performance,[1,4] relatively prohibitive cost and low-abundance of these materials limit their large-scale applications.[3] Development of non-noble metal based nonenzymatic electrochemical glucose sensors have thus garnered significant interest in recent years.[3,7−11]

Metal−organic frameworks (MOFs), as a class of organic−inorganic hybrid materials with well-ordered tunable porous structures, high internal surface area, and good thermal and chemical stability, have drawn much attention in gas storage, separation, energy storage and conversion, and sensors.[12−22] Although MOFs have abundant intrinsic molecular metal sites, they are generally recognized as poor electrode materials due to the natures of poor conductivity and relatively small pore size.[17,23,24] Some recently proposed effective strategies to resolve these problems could be mainly divided into five aspects: (i) High-temperature calcinations of MOFs to be more porous metal alloys/C, metal oxides, or metal oxides/C.[25−28] (ii) Hybridization MOFs with other conductive materials like graphene, MoS$_2$, atomically dispersed metals, metal hydroxides, or polymers.[29−33] (iii) Turning MOFs into ultrathin 2D nanosheets with coordinately unsaturated metal sites and fast electron-transfer kinetics.[34−36] (iv) Topological conversion of MOFs into more porous and conductive metal

Received: April 22, 2018

DOI: 10.1021/acs.inorgchem.8b01106

phosphides and chalcogenides.[37−41] (v) Fabrication of well-aligned 3D MOFs architectures with more exposed active sites, larger electrolyte/catalyst contact area, and faster transportation of active species than powder ones.[17,23,42−46]

However, considering that the calcination and topological conversion may sacrifice MOFs' intrinsic molecular metal active sites and combination with other materials may block the intrinsic micropores,[17,23,24] synthesis of MOFs with ultrathin 2D or well-aligned 3D nanostructures are thus considered ideal solutions to endow MOFs with more active sites and faster electron transfer. Moreover, it should be noted that ultrathin 2D MOF nanosheets still need the time-consuming post-coating procedures with polymeric binders during the electrode preparation, which would inevitably reduce the active surface area and cause potential peeling off of catalysts during long-time gas evolution.[47] In comparison, direct growth of well-aligned open-shelled MOF nanoarrays on current collectors, as a facile binder-free synthetic scheme, could guarantee the sufficient catalysts/electrolyte contact, favorable electric conductivity, and mechanical stability.[25] Carbon cloth is a type of cheap and commercially available textile with high conductivity, excellent flexibility, robust corrosion resistance, and strong mechanical strength, representing an ideal 3D substrate to integrate catalysts for electrocatalysis.[48]

Besides, as a typical subclass of MOFs with a tetrahedral network structurally similar to the aluminosilicate zeolites, zeolitic imidazolate frameworks (ZIFs) that consist of transition-metal cations (M) and imidazole-based ligands (Im) have been widely used in hydrogen storage, CO_2 capture/conversion, and heterogeneous catalysis, due to their good thermal and chemical stability, microporous structure, large surface area, and tunable pore aperture.[49] Among different kind of ZIFs, ZIF-67, which is composed of Co^{2+} and 2-methylimidazole, has caused particular interest in the design of electrode materials for electrocatalysis or batteries.[49] However, there are limited reported works on using ZIF-67 directly as electrodes,[50−52] and all the catalysts are in the form of powders with sodalite topology and a space group of $I43m$.[53] Another kind of 2D ZIF-67, ZIF-L, with a leaf-like structure and confirmed good photocatalytic activity,[53] has not been even reported as electrode materials.

With these understandings, we verified here that a leaf-like ZIF-L nanosheet array assembled on the carbon cloth (denoted as Co-MOF NS/CC) synthesized by a facile ambient liquid-phase deposition could act as a versatile electrocatalyst for glucose and water oxidation. Experimental results indicate that it not only exhibits good glucose-sensing performance with low determination limit and large detection range, but has high water-oxidation efficiency with low overpotential and good durability. These good performances could be ascribed to the enlarged catalyst/electrolyte contact area and exposed enough active sites enabled by the 3D well-aligned nanoarray, as well as the native good catalytic activity of Co-MOFs.

■ RESULTS AND DISCUSSION

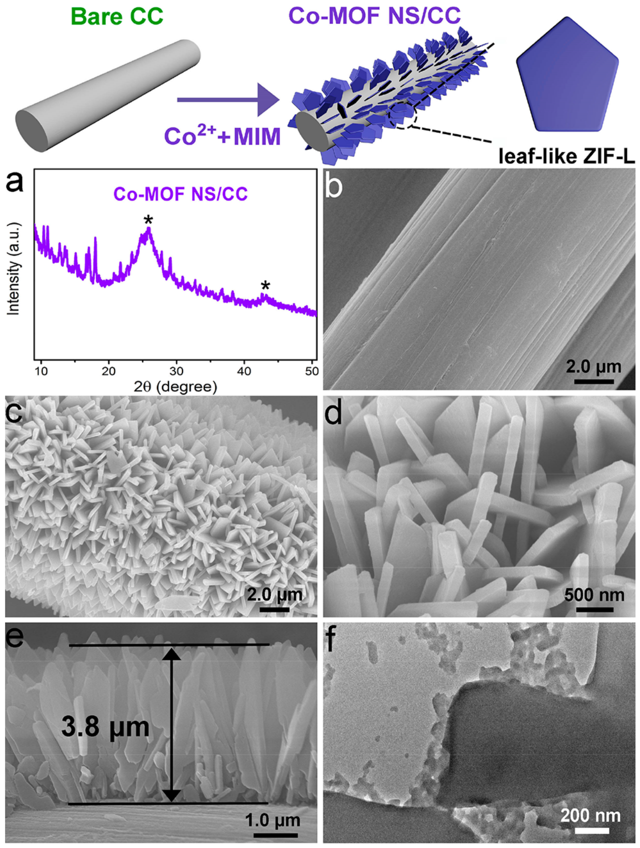

Figure 1. Top: Schematic illustration for the fabrication of Co-MOF NS/CC. (a) XRD pattern of Co-MOF NS/CC. (b) SEM image of the bare CC. (c,d) Low- and high-resolution SEM images of Co-MOF NS/CC. (e) Cross-sectional SEM image of Co-MOF NS/CC; (f) TEM image of the scratched Co-MOF nanosheet.

The fabrication process of Co-MOF NS/CC is illustrated in the top portion of Figure 1. The optical photograph of color change from bare CC to Co-MOF NS/CC and detailed description are shown in the Supporting Information. Figure 1a shows the X-ray diffraction (XRD) pattern of Co-MOF NS/CC. Except for the two typical broad peaks located at about 26 and 43° ascribing to the substrate of CC (marked with the five-pointed star),[48] other peaks match well with the diffraction pattern of reported leaf-like ZIF-67 (also denoted as ZIF-L).[53,54] The ZIF-L exhibits a different crystal structure with a space group of *Cmce* compared with previously reported ZIF-67 materials with sodalite topology and a space group of $I43m$.[53,54] Figures 1b and S2a show the field emission scanning electron microscopy (FE-SEM) images of bare carbon cloth. After deposition with Co-MOF, the skeleton of carbon fibers is fully covered with their well-aligned nanoarrays (Figures 1c and S2b). Closer longitudinal and cross-sectional views (Figure 1d,e) indicate these units are actually leaf-like smooth nanosheets with the thickness of 160 nm and the height of 3.8 μm. Elemental mapping images prove the presence and uniform distribution of Co, C, N, and O elements on the Co-MOF NS/CC (Figure S3). Transmission electron microscope (TEM) image (Figure 1f) of Co-MOF phase scratched from CC further shows a well-defined nanosheet morphology. N_2 adsorption/desorption isotherms and multipoint Brunauer−Emmett−Teller (BET) plot of the scratched Co-MOF nanosheets show that it has a BET surface area of 17.08 m^2 g^{-1} (Figure S4a,b), consistent well with the reported value of 16.245 m^2 g^{-1} for ZIF-L.[53] This result suggests the as-synthesized Co-MOF nanosheets have no channels owing to the leaf-like morphology with a 2D laminated structure.[54] The surface elemental compositions and valence states of Co-MOF NS/CC were further analyzed by the X-ray photoelectron spectroscopy (XPS). Survey XPS spectrum proves the existence of Co, C, N, and O elements in Co-MOF NS/CC

(Figure S5a), consistent with above-mentioned elemental mapping results. Figure S5b,c show the high-resolution XPS spectra of Co 2p and N 1s. The XPS spectrum of Co 2p shows Co $2p_{3/2}$ and Co $2p_{1/2}$ peaks centered at 781.2 and 796.7 eV, respectively, along with two shakeup satellites (identified as "Sat.") at 786.3 and 802.5 eV, indicating that the Co^{2+} state is predominant in Co-MOF phase.[55] The N 1s spectrum shows two peaks centered at about 398.8 and 400.3 eV, which could be well assigned to the pyridinic N and pyrrolic N, respectively.[56]

The glucose-sensing performances of Co-MOF NS/CC, Co-MOF NS powder/CC and bare CC were investigated via cyclic voltammetry (CV) in 0.1 M NaOH in the absence and presence of 1.0 mM glucose at a scan rate of 50 mV s^{-1} (Figure 2a). In the absence of glucose, there is no any redox peak for bare CC (black dotted line). In contrast, a pair of redox peaks for both the Co-MOF NS/CC (violet dotted line) and Co-MOF NS powder/CC (green dotted line) can be obviously observed. When 1.0 mM glucose was added in above electrolyte, bare CC causes a negligible oxidation current density (black solid line), while significant increases in anodic peak current density for both the Co-MOF NS/CC (violet solid line) and Co-MOF NS powder/CC (green solid line) could be clearly seen. This phenomenon suggests the Co-MOF phase possesses high electrocatalytic activity for glucose oxidation. Besides, from the bar chart of comparison of current density increments for different electrodes (inset in Figure 2a), we could concluded that the Co-MOF NS/CC has a higher glucose-oxidation performance than Co-MOF NS powder/CC, indicating that the integrated nanoarray structure is beneficial to the improved catalytic performance of Co-MOF NS/CC. In addition, the cyclic voltammetric curves (CVs) of Co-MOF NS/CC in 0.1 M NaOH containing 1.0 mM glucose at different scan rates were also acquired, as depicted in Figure S6a. It can be seen that the anodic peak shows a slightly positive shift and the cathodic peak shifts negatively with the increase of scan rate. Figure S6b exhibits that both the anodic and cathodic peak current densities increase linearly with the scan rates in the range of 30−100 mV s^{-1}. The good linear relationship between peak current densities and scan rates implies a diffusion-controlled electrochemical process of glucose oxidation on the surface of Co-MOF NS/CC.[8,57]

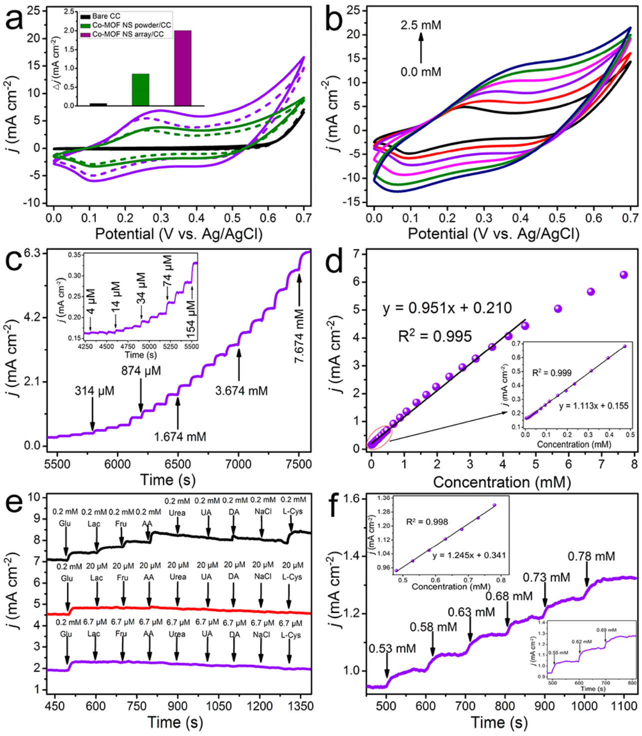

Figure 2. (a) CVs of bare CC (black curves), Co-MOF NS powder/CC (green curves), and Co-MOF NS array/CC (violet curves) in 0.1 M NaOH with and without the presence of 1.0 mM glucose at 50 mV s^{-1}. Inset: bar chart of comparison of current density increments for different electrodes. (b) CVs of Co-MOF NS/CC in 0.1 M NaOH with different glucose concentrations (0−2.5 mM) at 50 mV s^{-1}. (c) Amperometric responses of Co-MOF NS/CC to the successive addition of glucose at 0.5 V vs Ag/AgCl (Inset is the *i*−*t* curve at low glucose concentration range). (d) Corresponding linear calibration curve. Inset is amplification of the calibration curve in the low glucose concentration range. (e) Amperometric responses of the Co-MOF NS/CC toward the successive addition of different concentrations of glucose, Lac, Fru, AA, Urea, UA, DA, NaCl, and L-Cys in a stirred 0.1 M NaOH. (f) Amperometric responses of the Co-MOF NS/CC with the successive addition of 0.05 mM glucose in 10% diluted human blood serum sample. Inset in the top left corner: Corresponding calibration curve. Inset in the lower right corner: amperometric responses of this sensor with the successive addition of another glucose concentration of 0.07 mM in a new 10% diluted serum sample.

To further study the sensing performance of Co-MOF NS/CC electrode toward nonenzymatic glucose detection, CVs of the Co-MOF NS/CC electrode in 0.1 M NaOH containing different concentrations of glucose were recorded here (Figure 2b). As observed, the anodic peak current densities increase with the increase of glucose concentration in the range of 0−2.5 mM. A good linear correlation between glucose concentrations and anodic peak current densities in the whole concentration range (0−2.5 mM) can be obtained (Figure S7). These results indicate the excellent catalytic performance of Co-MOF NS/CC for glucose oxidation.

The optimal application potential was further tested by dropwise addition of 1.0 mM glucose to 0.1 M NaOH at 100 s interval under different potentials in the range of 0.30−0.55 V, as presented in Figure S8. When the potential is 0.50 V, the current density reaches the top and the signal-to-noise ratio is relatively small. No matter the potential is higher or lower than 0.50 V, the current density will decrease. Therefore, we chose 0.50 V as the optimal working potential in the follow-up experiments. Amperometric responses to successive injection of different glucose concentrations in constantly stirred 0.1 M NaOH were also performed. As shown in Figure 2c, amperometric current density response increases with the continuous addition of glucose. The lowest response concentration of 4 μM (determination limit, LOD) can be seen in the inset. Figure 2d displays excellent linearity between the steady-state current densities and glucose concentrations in the range of 0.004−4.428 mM, and a relative-high sensitivity of 1113 μA mM^{-1} cm^{-2} calculated by the slope (inset). The limit of detection was calculated to be 1.2 μM by using the equation of LOD = 3.3 σ/S, where σ is the standard deviation of intercept and S is the slope of the calibration curve.[4] However, the limit of detection just reflects theoretically the minimum detectable concentration. In contrast, determination limit is more reliable and meaningful that it could provide an accurate minimum detectable concentration.[4] Quantitative comparisons in regard to linear range, LOD, and sensitivity of this electrode with other reported superior transition-metal based glucose

DOI: 10.1021/acs.inorgchem.8b01106

sensors were presented in Table S1, proving its superiority in glucose sensing.

The selectivity and practical feasibility in diluted human blood serum of this sensor were further tested. Figure 2e exhibits the amperometric response of the Co-MOF NS/CC at 0.5 V to the successive addition of different concentrations of interferents and glucose in a stirred 0.1 M NaOH. With stepwise addition of the same concentration (0.2 mM), obvious current responses of these interferents could be seen (black curve). As the glucose concentration in human serum is generally about 30 times higher than those for other interferents,[4] the concentration ratios of these interferents and glucose at 1:10 and 1:30 (physiological level) were applied for comparison. It could be seen that these interfering species (20 or 6.7 μM) cause negligible current responses, proving the excellent selectivity of Co-MOF NS/CC for glucose under physiological conditions. We also applied this sensor in diluted human blood serum samples to verify its practicability for glucose sensing. Figure 2f shows the amperometric responses of Co-MOF NS/CC on the continuous addition of 0.05 mM glucose in 10% diluted human blood serum sample. Calibration curve (inset in the top left corner) shows that the current densities increase linearly with the increase of glucose concentrations from 0.48−0.78 mM. Furthermore, we recorded the amperometric responses with the successive addition of 0.07 mM glucose in another 10% diluted serum sample (inset in the lower right corner) and found that the glucose concentration is consistent well with the measured value in each sample with high recoveries from 100.4−103.4% (Table S2). The above results demonstrate this glucose sensor is feasible in diluted serums.

In addition to the glucose-sensing performance, the oxygen evolution reaction (OER) efficiency of Co-MOF NS/CC was also tested here to verify its good electrocatalytic-oxidation activity. The OER performances of Co-MOF NS/CC, Co-MOF NS powder/CC, bare CC, and RuO_2/CC were tested using linear sweep voltammetry (LSV) in a homemade three-electrode configuration with the electrodes as the working electrode, a graphite plate as the counter electrode, and a saturated calomel electrode (SCE) as the reference electrode. As shown in Figure 3a, Co-MOF NS/CC exhibits a higher current density and more negative OER onset potential (~1.52 V vs RHE) than Co-MOF NS powder/CC (~1.58 V vs RHE) and bare CC (~1.63 V vs RHE), although there is still a gap between RuO_2/CC and Co-MOF NS/CC. Note that the Co-MOF NS/CC has an obvious superiority over the calcined product of Co_3O_4 NS/CC (Figure S9) indicating that the calcination treatment will sacrifice this Co-MOF's intrinsic molecular metal active sites.[23,24] In addition, this Co-MOF NS/CC electrode shows small overpotentials of 330 and 370 mV to achieve current densities of 20 and 50 mA cm^{-2} with a relative-low Tafel slope of 106.6 mV dec^{-1} (Figure 3a,b), surpassing those for Co-MOF NS powder/CC and some newly reported MOF-based catalysts and even some transition metal based oxides, hydroxides, chalcogenides, and phosphides (Table S3). Both the small overpotential and low Tafel slope demonstrate this Co-MOF NS/CC possesses a high activity and fast reaction kinetics for OER.[58,59] To evaluate the stability of the Co-MOF NS/CC toward OER, multistep chronopotentiometric curve was also measured (Figure 3c). The Co-MOF NS/CC depicts an impressive OER durability with the polarization curve keeping almost the same after 5000 s electrolysis (inset in Figure 3c) and exhibits a fast amperometric response toward altered potentials with just needing less than 2 s to achieve a steady-state current density (inset), further proving the rapid reaction kinetics and excellent working stability of this Co-MOF NS/CC in base.[47,59,62]

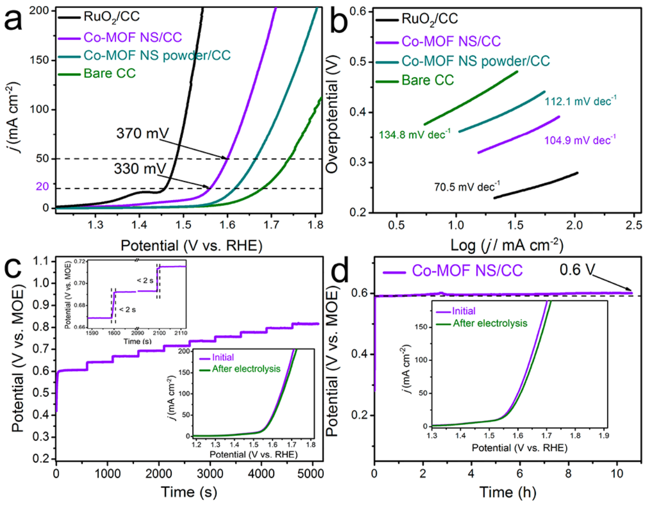

Figure 3. (a) LSV curves of RuO_2/CC, Co-MOF NS/CC, Co-MOF NS powder/CC, and bare CC at 2 mV s^{-1} in 1.0 M KOH. (b) Corresponding Tafel plots. (c) Multistep chronopotentiometric curve of Co-MOF NS/CC performed in 1.0 M KOH with anodic current densities increasing from 10 to 100 mA cm^{-2} (inset: response time and LSV curves before and after 5000 s durability test). (d) OER chronopotentiometric curve at a constant 10 mA cm^{-2} for Co-MOF NS/CC in 1.0 M KOH (inset: LSV curves before and after long-term durability test).

The long-term durability test shown in Figure 3d indicates the good stability of the Co-MOF NS/CC toward OER in 1.0 M KOH. The potential almost remains unchanged at the constant current density of 10 mA cm^{-2}, and the OER polarization curve after 10 h electrolysis shows negligible decay compared with the initial one (inset in Figure 3d). Of note, considering the zeolitic imidazolate framework (ZIF)-type MOFs are not stable in base, the Co-MOF might be converted to corresponding hydroxide or oxyhydroxide phases in the electro-oxidation process to sustain the stable OER catalysis. The SEM image, XRD pattern, XPS survey, and Co 2p spectra of the Co-MOF NS/CC after long-term OER test were recorded in Figure S10. The XRD pattern only exhibits the characteristic peaks of CC, possibly due to the conversion of Co-MOF to amorphous $Co(OH)_2$ or CoOOH. The recorded SEM image shows that the surface of Co-MOF nanosheets turns to be rough with many derived nanoparticles. XPS survey spectrum of Co-MOF after OER test shows that only small amounts of N element exists on the surface of this catalyst, further indicative of the conversion of Co-MOF to $Co(OH)_2$ or CoOOH phases. The XPS Co 2p spectrum shows that after electrolysis the Co^{2+} state in the catalyst turns to a mixed valence state of Co^{2+}/Co^{3+} with Co^{3+} state being predominant and demonstrates that the derived main phase is CoOOH. Besides, the flexural property of Co-MOF NS/CC was tested by deforming this electrode under various bending states. The photographs in Figure S11 indicate the Co-MOF NS/CC has a good mechanical flexibility.

The high catalytic activity toward both the OER and glucose oxidation of Co-MOF NS/CC could be well explained by the following four aspects of electrochemical surface area (ECSA), conductivity, unique open-shelled 3D nanoarrayed topology, and intrinsic catalytic activity of transition-metal based MOFs. First, the Nyquist curves in Figure 4a present that Co-MOF NS/CC has a smaller charge transfer resistance than Co-MOF NS powder/CC and bare CC, demonstrating the Co-MOF NS/CC possesses a more rapid electron transport kinetics.[25,32] Second, we compared the ECSAs of Co-MOF NS/CC, Co-MOF NS powder/CC, and bare CC (Figure S12) by double-layer capacitance (C_{dl}), which is typically used to represent ECSA.[58−65] Figure 4b indicates the C_{dl} value of Co-MOF NS/CC (192.5 mF cm^{-2}) is about 5 times larger than that for Co-MOF NS powder/CC (43.6 mF cm^{-2}) and 40 times larger than that for bare CC (4.88 mF cm^{-2}), proving the Co-MOF NS/CC owns a much higher ECSA than Co-MOF NS powder/CC and bare CC. Third, the well-aligned open-shelled nanoarrays structure provides a 3D mass-transfer pathway for electrolyte penetration and small molecules diffusion, and allows high utilization efficiency of catalytically active species.[25,48] Besides, the intrinsic high catalytic activity of Co-MOFs, which has been previously confirmed,[34,50−52] could also support the superior glucose and water oxidation activities of the Co-MOF NS/CC.

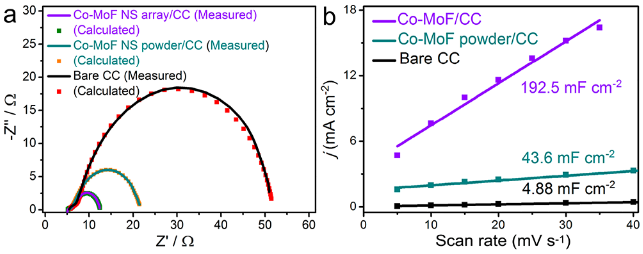

Figure 4. (a) Nyquist plots of Co-MOF NS/CC, Co-MOF NS powder/CC, and bare CC measured in 1.0 M KOH. (b) Capacitive current density (Δ*j*) at 0.15 V as a function of scan rate in the range of 0.1−0.2 V vs SCE.

■ CONCLUSION

In summary, we demonstrated here that the well-aligned Co-MOF NS/CC synthesized by a simple ambient liquid-phase deposition could act as a versatile anode for both glucose and water oxidation. Direct-growth of Co-MOF nanoarrays on CC not only reserves its intrinsic molecular metal active sites and micropores but also endows Co-MOF with some desired merits like large specific surface area, high conductivity, and efficient electrolyte/catalyst contact. Experimental data prove that the Co-MOF NS/CC has low determination limit and large detection range toward glucose sensing, and low overpotential and good durability toward water oxidation. This work not only demonstrates the potential of utilizing transition-metal based well-aligned MOF nanoarrays for sensing and water splitting but challenges a common conception that MOFs are inert catalysts for electrocatalytic reactions.

■ ASSOCIATED CONTENT

Ⓢ Supporting Information

The Supporting Information is available free of charge on the ACS Publications website at DOI: 10.1021/acs.inorg-chem.8b01106.

Methods; optical photographs; SEM images; elemental mappings; XPS spectra; electrochemical data; Tables S1−S3 (PDF)

■ AUTHOR INFORMATION

Corresponding Author

*E-mail: wanglong79@nwsuaf.edu.cn.

ORCID

Jianlong Wang: 0000-0002-2879-9489

Author Contributions

⊥Z.W. and W.Z. contributed equally to this work and are considered co-first authors.

Notes

The authors declare no competing financial interest.

■ ACKNOWLEDGMENTS

This work was supported by Grants from National Natural Science Foundation of China (Nos. 31701690, 21675127, and 31371813), the Fundamental Research Funds for the Central Universities (Nos. 2452015355, 2452017147, 2014YB093, and 2452015257), and the Development Project of Qinghai Key Laboratory (2017-ZJ-Y10).

■ REFERENCES

(1) Wang, J.; Thomas, D. F.; Chen, A. Nonenzymatic Electrochemical Glucose Sensor Based on Nanoporous PtPb Networks. *Anal. Chem.* **2008**, *80*, 997−1004.

(2) Cai, J.; Huang, J.; Ge, M.; Iocozzia, J.; Lin, Z.; Zhang, K.-Q.; Lai, Y. Immobilization of Pt Nanoparticles via Rapid and Reusable Electropolymerization of Dopamine on TiO_2 Nanotube Arrays for Reversible SERS Substrates and Nonenzymatic Glucose Sensors. *Small* **2017**, *13*, 1604240.

(3) Ci, S.; Huang, T.; Wen, Z.; Cui, S.; Mao, S.; Steeber, D. A.; Chen, J. Nickel Oxide Hollow Microsphere for Non-Enzyme Glucose Detection. *Biosens. Bioelectron.* **2014**, *54*, 251−257.

(4) Zhu, W.; Wang, J.; Zhang, W.; Hu, N.; Wang, J.; Huang, L.; Wang, R.; Suo, Y.; Wang, J. Monolithic Copper Selenide Submicron Particulates Film/Copper Foam Anode Catalyst for Ultrasensitive Electrochemical Glucose Sensing in Human Blood Serum. *J. Mater. Chem. B* **2018**, *6*, 718−724.

(5) Ko, Y.-S.; Kwon, Y.-U. Mesoporous Zirconia Thin Films with Three-Dimensional Pore Structures and their Application to Electrochemical Glucose Detection. *ACS Appl. Mater. Interfaces* **2013**, *5*, 3599−3606.

(6) Parlak, O.; İncel, A.; Uzun, L.; Turner, A. P. F.; Tiwari, A. Structuring Au Nanoparticles on Two-Dimensional MoS_2 Nanosheets for Electrochemical Glucose Biosensors. *Biosens. Bioelectron.* **2017**, *89*, 545−550.

(7) Chen, T.; Liu, D.; Lu, W.; Wang, K.; Du, G.; Asiri, A. M.; Sun, X. Three-dimensional Ni_2P Nanoarray: An Efficient Catalyst Electrode for Sensitive and Selective Nonenzymatic Glucose Sensing with High Specificity. *Anal. Chem.* **2016**, *88*, 7885−7889.

(8) Wang, Z.; Cao, X.; Liu, D.; Hao, S.; Du, G.; Asiri, A. M.; Sun, X. Ternary NiCoP Nanosheet Array on a Ti Mesh: A High-Performance Electrochemical Sensor for Glucose Detection. *Chem. Commun.* **2016**, *52*, 14438−14441.

(9) Xie, L.; Asiri, A. M.; Sun, X. Monolithically Integrated Copper Phosphide Nanowire: An Efficient Electrocatalyst for Sensitive and Selective Nonenzymatic Glucose Detection. *Sens. Actuators, B* **2017**, *244*, 11−16.

(10) Xie, F.; Liu, T.; Xie, L.; Sun, X.; Luo, Y. Metallic Nickel Nitride Nanosheet: An Efficient Catalyst Electrode for Sensitive and Selective Non-Enzymatic Glucose Sensing. *Sens. Actuators, B* **2018**, *255*, 2794−2799.

(11) Xie, F.; Cao, X.; Qu, F.; Asiri, A. M.; Sun, X. Cobalt Nitride Nanowire Array as an Efficient Electrochemical Sensor for Glucose and H_2O_2 Detection. *Sens. Actuators, B* **2018**, *255*, 1254−1261.

(12) Mason, J. A.; Veenstra, M.; Long, J. R. Evaluating Metal-Organic Frameworks for Natural Gas Storage. *Chem. Sci.* **2014**, *5*, 32−51.

(13) Rodenas, T.; Luz, I.; Prieto, G.; Seoane, B.; Miro, H.; Corma, A.; Kapteijn, F.; Llabres i Xamena, F. X.; Gascon, J. Metal-Organic Framework Nanosheets in Polymer Composite Materials for Gas Separation. *Nat. Mater.* **2015**, *14*, 48−55.

(14) Hu, H.; Guan, B.; Xia, B.; Lou, X. W. Designed Formation of $Co_3O_4/NiCo_2O_4$ Double-Shelled Nanocages with Enhanced Pseudo-capacitive and Electrocatalytic Properties. *J. Am. Chem. Soc.* **2015**, *137*, 5590−5595.

(15) Mahmood, A.; Guo, W.; Tabassum, H.; Zou, R. Metal-Organic Framework-Based Nanomaterials for Electrocatalysis. *Adv. Energy Mater.* **2016**, *6*, 1600423.

(16) Wu, H. B.; Lou, X. W. Metal-Organic Frameworks and Their Derived Materials for Electrochemical Energy Storage and Conversion: Promises and Challenges. *Sci. Adv.* **2017**, *3*, eaap9252.

(17) Deng, T.; Zhang, W.; Arcelus, O.; Wang, D.; Shi, X.; Zhang, X.; Carrasco, J.; Rojo, T.; Zheng, W. Vertically Co-Oriented Two Dimensional Metalorganic Frameworks for Packaging Enhanced Supercapacitive Performance. *Commun. Chem.* **2018**, *1*, 6.

(18) Guan, B. Y.; Yu, X. Y.; Wu, H. B.; Lou, X. W. Complex Nanostructures from Materials Based on Metal-Organic Frameworks for Electrochemical Energy Storage and Conversion. *Adv. Mater.* **2017**, *29*, 1703614.

(19) Xia, W.; Mahmood, A.; Zou, R.; Xu, Q. Metal-Organic Frameworks and their Derived Nanostructures for Electrochemical Energy Storage and Conversion. *Energy Environ. Sci.* **2015**, *8*, 1837−1866.

(20) Liu, H.; Xu, C.; Li, D.; Jiang, H.-L. Photocatalytic Hydrogen Production Coupled with Selective Benzylamine Oxidation over MOF Composites. *Angew. Chem., Int. Ed.* **2018**, *57*, 5379−5383.

(21) Wen, H.-M.; Li, B.; Li, L.; Lin, R.-B.; Zhou, W.; Qian, G.; Chen, B. A Metal-Organic Framework with Optimized Porosity and Functional Sites for High Gravimetric and Volumetric Methane Storage Working Capacities. *Adv. Mater.* **2018**, *30*, 1704792.

(22) Yassine, O.; Shekhah, O.; Assen, A. H.; Belmabkhout, Y.; Salama, K. N.; Eddaoudi, M. H_2S Sensors: Fumarate-Based fcu-MOF Thin Film Grown on a Capacitive Interdigitated Electrode. *Angew. Chem., Int. Ed.* **2016**, *55*, 15879−15883.

(23) Duan, J.; Chen, S.; Zhao, C. Ultrathin Metal-Organic Framework Array for Efficient Electrocatalytic Water Splitting. *Nat. Commun.* **2017**, *8*, 15341.

(24) Jia, H.; Yao, Y.; Zhao, J.; Gao, Y.; Luo, Z.; Du, P. A Novel Two-Dimensional Nickel Phthalocyanine-Based Metal-Organic Framework for Highly Efficient Water Oxidation Catalysis. *J. Mater. Chem. A* **2018**, *6*, 1188−1195.

(25) Xu, H.; Shi, Z.; Tong, Y.; Li, G. Porous Microrod Arrays Constructed by Carbon-Confined NiCo@ $NiCoO_2$ Core@Shell Nanoparticles as Efficient Electrocatalysts for Oxygen Evolution. *Adv. Mater.* **2018**, *30*, 1705442.

(26) Lu, X.; Gu, L.; Wang, J.; Wu, J.; Liao, P.; Li, G. Bimetal-Organic Framework Derived $CoFe_2O_4$/C Porous Hybrid Nanorod Arrays as High-Performance Electrocatalysts for Oxygen Evolution Reaction. *Adv. Mater.* **2017**, *29*, 1604437.

(27) Ma, T. Y.; Dai, S.; Jaroniec, M.; Qiao, S. Z. Metal-Organic Framework Derived Hybrid Co_3O_4-Carbon Porous Nanowire Arrays as Reversible Oxygen Evolution Electrodes. *J. Am. Chem. Soc.* **2014**, *136*, 13925−13931.

(28) Guan, C.; Liu, X.; Ren, W.; Li, X.; Cheng, C.; Wang, J. Rational Design of Metal-Organic Framework Derived Hollow $NiCo_2O_4$ Arrays for Flexible Supercapacitor and Electrocatalysis. *Adv. Energy Mater.* **2017**, *7*, 1602391.

(29) Xia, W.; Qu, C.; Liang, Z.; Zhao, B.; Dai, S.; Qiu, B.; Jiao, Y.; Zhang, Q.; Huang, X.; Guo, W.; Dang, D.; Zou, R.; Xia, D.; Xu, Q.; Liu, M. High-Performance Energy Storage and Conversion Materials Derived from a Single Metal-Organic Framework/Graphene Aerogel Composite. *Nano Lett.* **2017**, *17*, 2788−2795.

(30) Ren, W.; Zhang, H.; Guan, C.; Cheng, C. Ultrathin MoS_2 Nanosheets@Metal Organic Framework-Derived N-Doped Carbon Nanowall Arrays as Sodium Ion Battery Anode with Superior Cycling Life and Rate Capability. *Adv. Funct. Mater.* **2017**, *27*, 1702116.

(31) Liang, Z.; Qu, C.; Xia, D.; Zou, R.; Xu, Q. Atomically Dispersed Metal Sites in MOF-Based Materials for Electrocatalytic and Photocatalytic Energy Conversion. *Angew. Chem.* **2018**, DOI: 10.1002/ange.201800269.

(32) Wu, D.; Wei, Y.; Ren, X.; Ji, X.; Liu, Y.; Guo, X.; Liu, Z.; Asiri, A. M.; Wei, Q.; Sun, X. $Co(OH)_2$ Nanoparticle-Encapsulating Conductive Nanowires Array: Room-Temperature Electrochemical Preparation for High-Performance Water Oxidation Electrocatalysis. *Adv. Mater.* **2018**, *30*, 1705366.

(33) Wang, L.; Feng, X.; Ren, L.; Piao, Q.; Zhong, J.; Wang, Y.; Li, H.; Chen, Y.; Wang, B. Flexible Solid-State Supercapacitor Based on a Metal-Organic Framework Interwoven by Electrochemically-Deposited PANI. *J. Am. Chem. Soc.* **2015**, *137*, 4920−4923.

(34) Zhao, S.; Wang, Y.; Dong, J.; He, C.; Yin, H.; An, P.; Zhang, X.; Zhao, K.; Gao, C.; Zhang, L.; et al. Ultrathin Metal-Organic Framework Nanosheets for Electrocatalytic Oxygen Evolution. *Nat. Energy* **2016**, *1*, 16184.

(35) Hai, G.; Jia, X.; Zhang, K.; Liu, X.; Wu, Z.; Wang, G. High-Performance Oxygen Evolution Catalyst Using Two-Dimensional Ultrathin Metal-Organic Frameworks Nanosheets. *Nano Energy* **2018**, *44*, 345−352.

(36) Huang, J.; Li, Y.; Huang, R.; He, C.; Gong, L.; Hu, Q.; Wang, L.; Xu, Y.; Tian, X.; Liu, S.-Y.; et al. Electrochemical Exfoliation of Pillared-Layer Metal-Organic Framework to Boost the Oxygen Evolution Reaction. *Angew. Chem.* **2018**, *130*, 4722−4726.

(37) Jiao, L.; Zhou, Y.; Jiang, H. Metal-Organic Framework-Based CoP/Reduced Graphene Oxide: High-Performance Bifunctional Electrocatalyst for Overall Water Splitting. *Chem. Sci.* **2016**, *7*, 1690−1695.

(38) He, P.; Yu, X.; Lou, X. W. Carbon-Incorporated Nickel-Cobalt Mixed Metal Phosphide Nanoboxes with Enhanced Electrocatalytic Activity for Oxygen Evolution. *Angew. Chem.* **2017**, *129*, 3955−3958.

(39) Jayaramulu, K.; Masa, J.; Tomanec, O.; Peeters, D.; Ranc, V.; Schneemann, A.; Zboril, R.; Schuhmann, W.; Fischer, R. A. Nanoporous Nitrogen-Doped Graphene Oxide/Nickel Sulfide Composite Sheets Derived from a Metal-Organic Framework as an Efficient Electrocatalyst for Hydrogen and Oxygen Evolution. *Adv. Funct. Mater.* **2017**, *27*, 1700451.

(40) He, W.; Ifraemov, R.; Raslin, A.; Hod, I. Room-Temperature Electrochemical Conversion of Metal-Organic Frameworks into Porous Amorphous Metal Sulfides with Tailored Composition and Hydrogen Evolution Activity. *Adv. Funct. Mater.* **2018**, *28*, 1707244.

(41) Xu, X.; Liu, J.; Liu, J.; Ouyang, L.; Hu, R.; Wang, H.; Yang, L.; Zhu, M. A General Metal-Organic Framework (MOF)-Derived Selenidation Strategy for In Situ Carbon-Encapsulated Metal Selenides as High-Rate Anodes for Na-Ion Batteries. *Adv. Funct. Mater.* **2018**, *28*, 1707573.

(42) Cai, G.; Zhang, W.; Jiao, L.; Yu, S.; Jiang, H. Template-Directed Growth of Well-Aligned MOF Arrays and Derived Self-Supporting Electrodes for Water Splitting. *Chem.* **2017**, *2*, 791−802.

(43) Deng, T.; Lu, Y.; Zhang, W.; Sui, M.; Shi, X.; Wang, D.; Zheng, W. Inverted Design for High-Performance Supercapacitor Via $Co(OH)_2$-Derived Highly Oriented MOF Electrodes. *Adv. Energy Mater.* **2018**, *8*, 1702294.

(44) Li, W.; Ding, K.; Tian, H.; Yao, M.; Nath, B.; Deng, W.; Wang, Y.; Xu, G. Conductive Metal-Organic Framework Nanowire Array Electrodes for High-Performance Solid-State Supercapacitors. *Adv. Funct. Mater.* **2017**, *27*, 1702067.

(45) Xie, M.; Xiong, X.; Yang, L.; Shi, X.; Asiri, A. M.; Sun, X. An $Fe(TCNQ)_2$ Nanowire Array on Fe Foil: An Efficient Non-Noble-Metal Catalyst for the Oxygen Evolution Reaction in Alkaline Media. *Chem. Commun.* **2018**, *54*, 2300−2303.

(46) Lu, W.; Wu, X. Ni-MOF Nanosheet Arrays: Efficient Non-Noble-Metal Electrocatalysts for Non-Enzymatic Monosaccharide Sensing. *New J. Chem.* **2018**, *42*, 3180−3183.

(47) Zhu, W.; Yue, Z.; Zhang, W.; Hu, N.; Luo, Z.; Ren, M.; Xu, Z.; Wei, Z.; Suo, Y.; Wang, J. Wet-Chemistry Topotactic Synthesis of Bimetallic Iron-Nickel Sulfide Nanoarrays: An Advanced and Versatile Catalyst for Energy Efficient Overall Water and Urea Electrolysis. *J. Mater. Chem. A* **2018**, *6*, 4346−4353.

(48) Zhu, W.; Ren, M.; Hu, N.; Zhang, W.; Luo, Z.; Wang, R.; Wang, J.; Huang, L.; Suo, Y.; Wang, J. Traditional $NiCo_2S_4$ Phase with Porous Nanosheets Array Topology on Carbon Cloth: A Flexible, Versatile and Fabulous Electrocatalyst for Overall Water and Urea Electrolysis. *ACS Sustainable Chem. Eng.* **2018**, *6*, 5011−5020.

(49) Zhong, G.; Liu, D.; Zhang, J. The Application of ZIF-67 and its Derivatives: Adsorption, Separation, Electrochemistry and Catalysts. *J. Mater. Chem. A* **2018**, *6*, 1887−1899.

(50) Xu, Q.; Li, H.; Yue, F.; Chi, L.; Wang, J. Nanoscale Cobalt Metal-Organic Framework as a Catalyst for Visible Light-Driven and Electrocatalytic Water Oxidation. *New J. Chem.* **2016**, *40*, 3032−3035.

(51) Wang, S.; Hou, Y.; Lin, S.; Wang, X. Water Oxidation Electrocatalysis by a Zeolitic Imidazolate Framework. *Nanoscale* **2014**, *6*, 9930−9934.

(52) Meng, W.; Wen, Y.; Dai, L.; He, Z.; Wang, L. A Novel Electrochemical Sensor for Glucose Detection Based on Ag@ZIF-67 Nanocomposite. *Sens. Actuators, B* **2018**, *260*, 852−860.

(53) Wang, M.; Liu, J.; Guo, C.; Gao, X.; Gong, C.; Wang, Y.; Liu, B.; Li, X.; Gurzadyan, G. G.; Sun, L. Metal-Organic Frameworks (ZIF-67) as Efficient Cocatalysts for Photocatalytic Reduction of CO_2: the Role of the Morphology Effect. *J. Mater. Chem. A* **2018**, *6*, 4768−4775.

(54) Chen, R.; Yao, J.; Gu, Q.; Smeets, S.; Baerlocher, C.; Gu, H.; Zhu, D.; Morris, W.; Yaghi, O. M.; Wang, H. A Two-Dimensional Zeolitic Imidazolate Framework with a Cushion-Shaped Cavity for CO_2 Adsorption. *Chem. Commun.* **2013**, *49*, 9500−9502.

(55) Hu, X.; Hu, H.; Li, C.; Li, T.; Lou, X.; Chen, Q.; Hu, B. Cobalt-Based Metal Organic Framework with Superior Lithium Anodic Performance. *J. Solid State Chem.* **2016**, *242*, 71−76.

(56) Hou, Y.; Li, J.; Wen, Z.; Cui, S.; Yuan, C.; Chen, J. Co_3O_4 Nanoparticles Embedded in Nitrogen-Doped Porous Carbon Dodecahedrons with Enhanced Electrochemical Properties for Lithium Storage and Water Splitting. *Nano Energy* **2015**, *12*, 1−8.

(57) Zhang, Y.; Zhao, D.; Zhu, W.; Zhang, W.; Yue, Z.; Wang, J.; Wang, R.; Zhang, D.; Wang, J.; Zhang, G. Engineering Multi-Stage Nickel Oxide Rod-on-Sheet Nanoarrays on Ni Foam: A Superior Catalytic Electrode for Ultrahigh-Performance Electrochemical Sensing of Glucose. *Sens. Actuators, B* **2018**, *255*, 416−423.

(58) Ji, X.; Zhang, R.; Shi, X.; Asiri, A. M.; Zheng, B.; Sun, X. Fabrication of Hierarchical CoP Nanosheet@Microwire Arrays via Space-Confined Phosphidation toward High-Efficiency Water Oxidation Electrocatalysis under Alkaline Conditions. *Nanoscale* **2018**, *10*, 7941−7945.

(59) Zhu, W.; Liu, L.; Yue, Z.; Zhang, W.; Yue, X.; Wang, J.; Yu, S.; Wang, L.; Wang, J. Au Promoted Nickel-Iron Layered Double Hydroxide Nanoarrays: A Modular Catalyst Enabling High-Performance Oxygen Evolution. *ACS Appl. Mater. Interfaces* **2017**, *9*, 19807−19814.

(60) Yang, Q.; Wang, Y.; Wang, J.; Hu, N.; Liu, F.; Pei, H.; Yang, W.; Li, Z.; Suo, Y.; Wang, J. High Effective Adsorption/Removal of Illegal Food Dyes from Contaminated Aqueous Solution by Zr-MOFs. *Food Chem.* **2018**, *254*, 241−248.

(61) Wang, J.; Yang, Q.; Zhang, L.; Liu, M.; Hu, N.; Zhang, W.; Zhu, W.; Wang, R.; Suo, Y.; Wang, J. A Hybrid Monolithic Column Based on Layered Double Hydroxide-Alginate Hydrogel for Selective Solid Phase Extraction of Lead Ions in Food and Water Samples. *Food Chem.* **2018**, *257*, 155−162.

(62) He, L.; Zhou, D.; Lin, Y.; Ge, R.; Hou, X.; Sun, X.; Zheng, C. Ultra-Rapid In Situ Synthesis of Cu_2S Nanosheet Arrays on Copper Foam with Room Temperature Active Iodine Plasma for Efficient and Cost-Effective Oxygen Evolution. *ACS Catal.* **2018**, *8*, 3859−3864.

(63) Gou, Y.; Yang, L.; Liu, Z.; Asiri, A. M.; Hu, J.; Sun, X. $Cu_3Mo_2O_9$ Nanosheet Array as a High-Efficiency Oxygen Evolution Electrode in Alkaline Solution. *Inorg. Chem.* **2018**, *57*, 1220−1225.

(64) Xiong, X.; You, C.; Liu, Z.; Asiri, A. M.; Sun, X. Co-Doped CuO Nanoarray: An Efficient Oxygen Evolution Reaction Electrocatalyst with Enhanced Activity. *ACS Sustainable Chem. Eng.* **2018**, *6*, 2883−2887.

(65) Xiong, X.; Ji, Y.; Xie, M.; You, C.; Yang, L.; Liu, Z.; Asiri, A. M.; Sun, X. MnO_2-CoP_3 Nanowires Array: An Efficient Electrocatalyst for Alkaline Oxygen Evolution Reaction with Enhanced Activity. *Electrochem. Commun.* **2018**, *86*, 161−165.

DOI: 10.1021/acs.inorgchem.8b01106
Inorg. Chem. XXXX, XXX, XXX−XXX